Influence of the Substrate in the On-surface Synthesis and Air Stability of 1D Metal-Organic Oligomers

J. M. Gómez-Fernández[1], J. I. Martínez[1], J. M. Zamalloa-Serrano[1], T. Naranjo[2], C.G. López-Calixto[2], L. Schio[3], L. Floreano[3], I. Palacio[1], V. A. de la Peña O'Shea[2], M. Liras[2], J. A. Martín-Gago[1], M.F. López[1*], C. Sánchez-Sánchez[1*]*

[1] Instituto de Ciencia de Materiales de Madrid (ICMM-CSIC), C/Sor Juana Inés de la Cruz 3, 28049 Madrid (Spain)

[2] Photoactivated Processes Unit, IMDEA Energy Institute, Avda. Ramón de la Sagra 3, 28935 Móstoles, Madrid (Spain)

[3] Laboratorio TASC, CNR-IOM, Basovizza SS-14, Km 163.5, I-34149 Trieste (Italy)

Abstract

The development of applicable functional materials currently stands as one of the main challenges in the field of On-Surface Synthesis. In this direction, it is necessary to understand their stability in real conditions, what it is known as *bridging the pressure gap*. Interestingly, although it is well-established that the on-surface synthesis will be highly influenced by the selected substrate, little is known about the effect of the underlying substrate on the air stability of on-surface synthesized nanostructures. Applying an On-surface Synthesis approach, we report a similar behavior in the synthesis of 1D metal-organic nanostructures based on a BOPHY photoactive molecule on two coinage metal surfaces, Au(111) and Ag(111), but a distinct air stability of these nanostructures when exposed to the atmospheric pressure due to the different catalytic

properties of the substrates. In both cases, important comparative conclusions are extracted thanks to a combination of Surface Science characterization techniques with theoretical calculations. This study opens a door to the synthesis of low-dimensional photoactive materials with potential applications, emphasizing the critical role of the substrate not only in the synthesis process but also in the air stability of on-surface synthesized nanostructures.

Introduction

On-Surface Synthesis (OSS) has demonstrated its enormous potential for the bottom-up synthesis of a wide variety of atomically-precise materials at the nanoscale with exotic properties. This is achieved through the realization of chemical reactions catalyzed by the surfaces, which have been demonstrated to facilitate certain reactions by reducing the activation barriers. Additionally, OSS presents other unique characteristics that affords the synthesis of otherwise unattainable low dimensional nanostructures, like the use of controlled ultra-high vacuum (UHV) conditions that ensure an ultra-clean interface and a completely inert atmosphere, allowing the exploration of a wider temperature range before molecular degradation [1,2]. These ideal UHV conditions, together with the use of “perfect” single crystalline substrates and theoretical first-principles calculations, allow for the complete modeling and rationalization of their properties and the reaction mechanisms involved at the atomic and molecular scale. Thanks to this, a wide variety of novel 0D, 1D and 2D [3] nanostructures have been achieved, demonstrating the capabilities of this methodology to synthesize truly low-dimensional nanostructures just by properly selecting the organic precursor and the aimed reaction.

However, at the same time, those UHV conditions have kept this strategy far away from applications, with one of the great challenges of the field being the synthesis and application of truly functional materials. In this sense, some important efforts are being devoted in this direction, with keynote examples demonstrating the potential feasibility of applying those on-surface synthesized nanomaterials in technological applications, such as the fabrication of field effect transistors (FET) based on graphene nanoribbons [4], nitrogen-doped nanoporous graphene with prospective in photocatalytic and membrane applications [5], porphyrin-based nanostructures with potential applications in energy harvesting [6], or the achievement of a promising strategy to protect the reactive zigzag edges of chiral GNRs [7]. Nonetheless, there is still a long way to go. So far, most of the research in the field has been centered on the use of fully carbon-based precursors to yield graphene-based nanostructures given the "simplicity" and robustness of carbon-based chemistry, while little attention has been paid to more complex heteroatomic precursors that, indeed, can incorporate new functionalities. Even more, those heteroatomic precursors rarely go beyond three atomic species, without considering the H atoms (normally C, a halogen and a third atomic species, most typically N and, to a much lower extent, O, S, B or Si) [1].

In this sense, a particularly interesting molecule is the bis(difluoroboron)-1,2-bis-(pyrrol-2-yl)methylene-hydrazine (BOPHY) chromophore (Scheme 1). The BOPHY dye was first discover in 2014 simultaneously by two independent research groups [8,9]. Since then, its use has exponentially increased in different applications such as sensing [10–12], photosensitizer in photodynamic therapy [13,14], chemical actinometer [15], part of up conversion systems [16], and as the main moiety to prepare conjugated porous polymers CPPs [17–19] and covalent organic frameworks (COFs) for photocatalysis in

solar fuel production [20] or biomedical applications [21]. The BOPHY chromophore consists in four rings, with two pyrrole units at the periphery and two six-membered rings, each incorporating a N_2BF_2 group in opposite direction (5 and 10 positions). To increase its chemical stability, our target molecule is substituted by four bulky methyl group along its periphery. Additionally, to facilitate the formation of BOPHY-based nanostructures, our precursor monomer has been functionalized with I atoms at the *para* positions along the molecular longitudinal axis (I-BOPHY-I). In its solid state, the BOPHY chromophore is almost planar attending to x-ray diffraction measurements [8] but some authors suggested that, in solution, the real geometries of S0 and S1 electronic states are highly puckered [22], making interesting its study at the molecular level on a surface. Interestingly, the I-BOPHY-I molecule is prochiral, exhibiting adsorption-induced chirality when deposited on surfaces. The whole array of such molecular adsorbates is naturally racemic as spontaneous global mirror-symmetry breaking is disfavored [23].

In this work, we have applied the OSS approach to study the thermal behavior and air stability of the I-BOPHY-I molecule when deposited on two metal surfaces, Au(111) and Ag(111), while extracting valuable comparative conclusions on the role played by the substrate (see Scheme 1). Particularly, the surface is not only used as catalytic support, but also provides adatoms that play a crucial role in the formation of these metal-organic nanostructures, as well as in their air stability. Using powerful surface analysis techniques, such as scanning tunneling microscopy (STM) and X-ray photoelectron spectroscopy (XPS), combined with first-principles theoretical DFT calculations, we structurally and chemically unveil the obtained nanostructures and their evolution when exposed to air. This work evidences the remarkable potential of OSS as a powerful tool for the construction of truly low-dimensional functional materials with technological

interest and for the evaluation of the air stability of so-formed atomically-precise nanostructures.

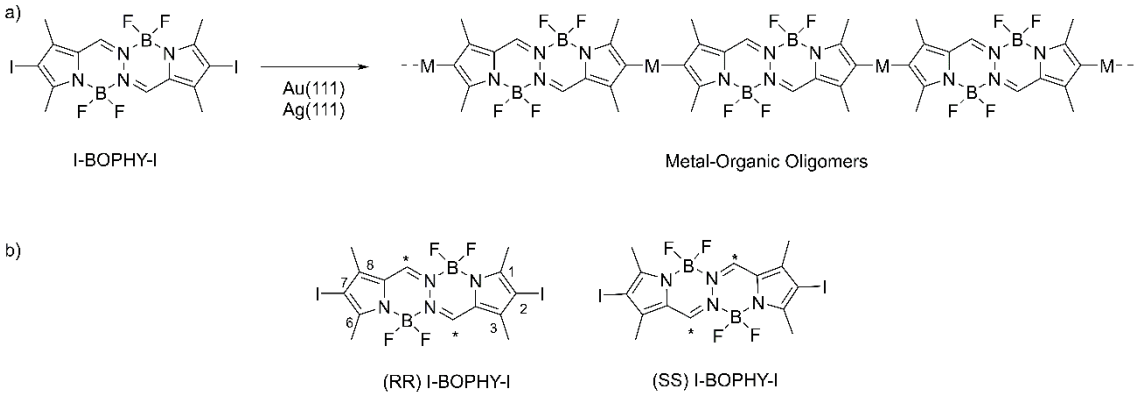

Scheme 1. a) Surface-assisted reaction of the I-BOPHY-I precursor on Au(111) and Ag(111) to form metal-organic oligomers by using the native metal adatoms characteristics of these surfaces. b) The I-BOPHY-I prochiral molecule. Note that (RR) and (SS) are considering as prochiral those C atoms on 4 and 9 positions.

Methods

The experiments were carried out in three different UHV systems, with a base pressure of low 10^{-10} mbar. Ag(111) and Au(111) single crystals (Mateck GmbH) were cleaned through repeated cycles of argon sputtering and annealing at 450°C before the evaporation of the molecules. The photoactive 2,7-diiodo-1,3,6,8-tetramethyl-bis(difluoroboron)-1,2-bis((1Hpyrrol-2-yl)methylene)hydrazine (from now on I-BOPHY-I) was synthesized in IMDEA-Energía following a previously described synthetic method and extra purified by sublimation [16–18]. After that, molecules were thermally sublimed onto metallic support using a quartz crucible held at 175°C and evaporation rate of 1 Å/min, as determined by a quartz crystal microbalance (Inficon). The BOPHY-based metal-organic nanostructures were prepared by thermal activation onto Ag(111) and Au(111) surfaces. Two different methods have been employed for the growth of the oligomers: i) precursor evaporation onto a hot surface and ii) precursor evaporation at

room temperature (RT) and stepwise annealing. Similar results have been obtained in both cases.

STM images were acquired in constant-current mode using a flow-cryostat low temperature scanning tunneling microscope LT-STM (STREAM SPM, Scienta Omicron) operated at 78K (LN_2) or 8K (LHe) under UHV conditions. WSxM software was used as a tool for data analysis [24].

The XPS measurements on Au(111) were performed at the ALOISA beamline of the Elettra synchrotron radiation facility in Trieste (Italy) [25]. The high-resolution XPS spectra were recorded with the analyzer oriented along the linearly polarized electric field while keeping the sample at a grazing incidence of 4.0˚ (close to normal emission and *p*-polarization). The electron spectrometer is a home-made hemispherical analyzer (mean radius of 66 mm) equipped with a high dynamic range (2 MHz) two-dimensional delay-line detector (2D-DLD) coupled to multi-channel plates. All spectra were acquired after I-BOPHY-I evaporation at RT and stepwise post-annealing at different temperatures. The photon energy used for the XPS measurements of F 1s and I 3d was 820 eV (overall XPS resolution better than 240 meV), while for C 1s and N 1s spectra was 515 eV (overall XPS resolution better than 160 meV). The scale in binding energy (BE) was calibrated to the Fermi level. We verified that no significant radiation damage took place on the timescale of the spectroscopic measurements by comparison of photoemission spectra measured on irradiated and fresh sample areas. XPS on Ag(111) and air stability measurements on Au(111) and Ag(111) were performed using a Phoibos 100 electron analyzer equipped with a 2D-DLD detector and an Al-Kα monochromatic X-Ray source.

The computational analysis of the different gas-phase systems and metal-organic interfacial phases was comprehensively conducted by using Density Functional Theory (DFT) as implemented within the localized basis set Gaussian16 [26] and the plane-wave QUANTUM ESPRESSO simulation packages [27]. Ground-state structures and electronic properties of molecular assemblies were computed using these theoretical frameworks, further employing the localized basis set FIREBALL code [28] for the simulation of Keldysh-Green STM-imaging (further details on the theoretical and computational methods are available in the Supporting Information).

Results

On-Surface I-BOPHY-I chemistry at the Au(111) metal interface

Figure 1a shows a STM image of the Au(111) surface after evaporation of I-BOPHY-I molecules at RT. As it can be observed, the molecular deposition leads to the formation of linear molecular rows that coexist with regions of apparently disordered molecular features (see black and green arrows, respectively). For the linear molecular arrangement, different domains, rotated by 120°, can be observed (compare regions of blue and black arrows), indicating a preferential molecular orientation associated to the characteristic three-fold symmetry of the substrate. A zoom of the STM image (Figure 1b) allow us to distinguish that these molecular rows are composed of double bright lobes. Two different characteristic lengths can be defined: 0.8 nm, corresponding to the separation between bright lobes within the rows, and 1.2 nm, between lobes of neighboring rows (red and black double arrows, respectively). Despite one could a priori be tempted to assign the lobes within rows to the molecular units, a careful analysis indicates the opposite. On the one hand, this separation (0.8 nm) is too small to accommodate a I-BOPHY-I molecule (1.3 nm) unless it is considered that the bright lobes

correspond to some internal molecular feature. On the other hand, when Figure 1a is analyzed in detail, it can be noticed that the edges of the ordered islands are composed by single lobe chains (see, for example, last row to the right of blue arrow). Thus, molecular units are assigned to lobes from neighboring rows. To corroborate our model, DFT theoretical calculations on the self-assembly of I-BOPHY-I molecules have been carried out. Figure S1 shows the result of such calculations, which unambiguously reinforce the validity of our model and indicate that the bright lobes correspond to the iodine atoms attached to the molecules.

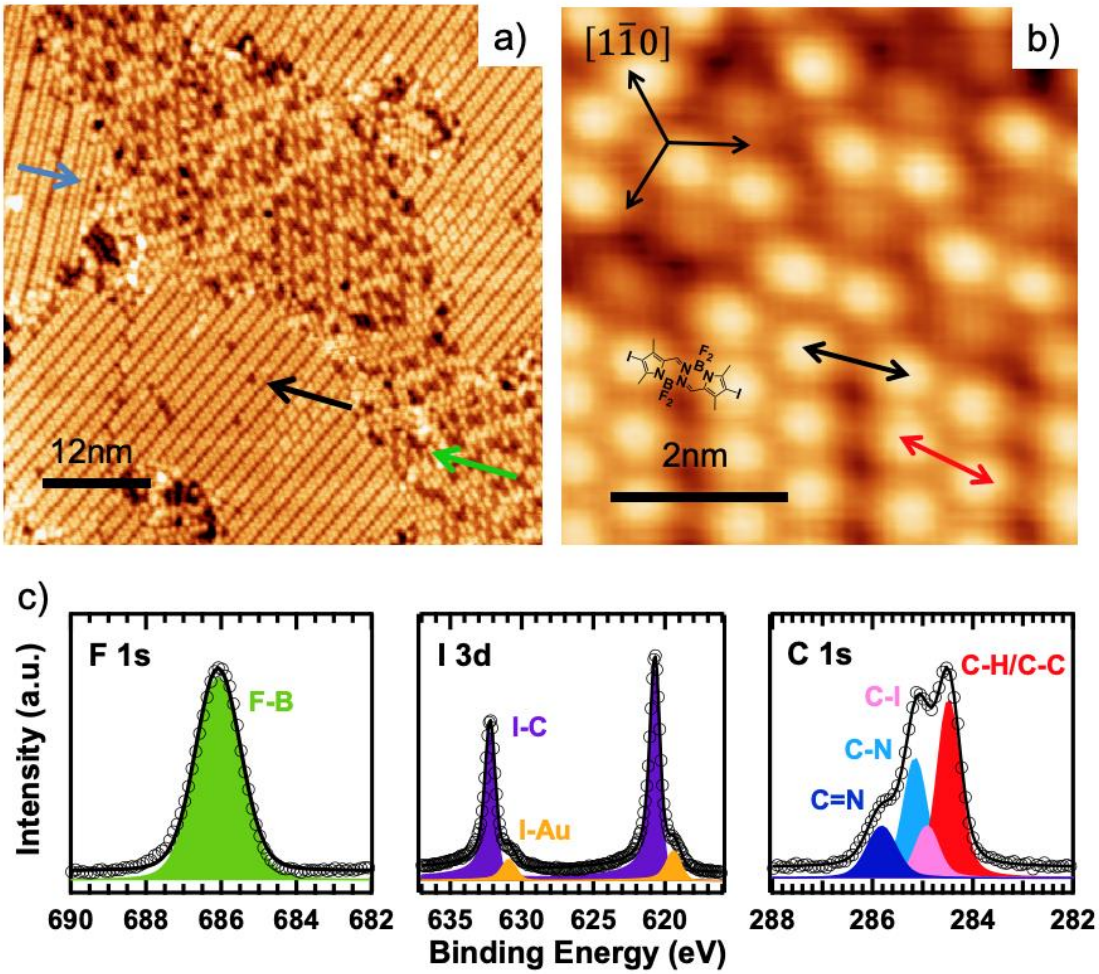

Figure 1. a) STM image after evaporation of I-BOPHY-I on Au (111) at RT, showing the different molecular arrangements: disorder region (green arrow) and self-assembled regions (black and blue arrows). b) HR-STM image of the self-assembled region. The set of three black arrows shows the main crystallographic directions of the Au(111) substrate. Red and black double arrows show the difference distances between

lobes. c) XPS spectra corresponding to F 1s, I 3d and C 1s regions. STM parameters: a) I_t=0.05 nA, V_b=1 V; b) I_t=0.05 nA, V_b=1 V.

At this point, it is interesting to note that, within the ordered phase, it is possible to distinguish two different assemblies (see Figure S2): homogeneous rows and bunched double rows (black and yellow arrows in Figure S2, respectively). It should be noted that the I-BOPHY-I is a prochiral molecule, thus, when deposited on the surface, it will express its chirality depending on the face in contact with the underlying metallic surface (see (RR or SS) I-BOPHY-I schematic representations in Figure S2a). Taking this into account, we attribute this different assembly to the chiral organization of the molecules. In the former case, the rows are homochiral, allowing for a denser packing due to the establishment of halogen bonds between the F atoms of neighboring molecules (see model in Figure S2c), while in the bunched case, a heterochiral arrangement stabilized by intermolecular F-H bonds occurs (Figure S2d). However, as it will be shown below, this prochirality will not play any role on the formation of the hybrid oligomers.

Regarding the apparently disordered area (green arrow), a non-homogeneous distribution of bright features (iodine atoms) can be observed. A separation between bright spots of around 2.6 nm (the double of the I-I distance in a I-BOPHY-I molecule) is observed, suggesting that they are the result of an intermolecular interaction between two partially dehalogenated molecules. Considering that a separation of ~2.3 nm is expected for a covalent I-BOPHY-BOPHY-I structure, the value of ~2.6 nm is attributed to a metal-organic dimer (I-BOPHY-M-BOPHY-I). To corroborate our assumption, we have simulated the STM images for metal-organic dimers, and an excellent agreement is achieved (see Figure S3). These results are also in good accordance with our XPS

results, as it will be shown below. Thus, these molecular structures would constitute the initial stages of the oligomer formation upon partial activation of the BOPHY molecules.

To better understand the chemical nature of the molecules on the Au(111) surface and to confirm the proposed models for the different nanostructures observed at RT, Figure 1c shows a set of XPS spectra for the F 1s, I 3d and C 1s core level peaks, while Table S1 presents the main parameters of the different components obtained from the fit analysis. The F 1s signal exhibits a single emission located at BE = 686.1 eV, corresponding to the F-B bond within the molecule [29]. In contrast, the I 3d spectrum is composed of two contributions: the main one ($3d_{5/2}$ at BE = 620.6 eV) corresponds to iodine in the I-BOPHY-I molecule, while the less intense emission, at BE = 619.3 eV, is assigned to iodine on the surface after partial molecular dehalogenation, in good agreement with literature [30]. Therefore, the larger contribution (purple curve) is ascribed to iodine present in the pristine molecules of the majority ordered phase and at the ends of the dimers. The smaller one (orange curve) corresponds to the iodine atoms detached from the molecules and stabilized on the metallic surface. Finally, the C 1s XPS emission shows four different components corresponding to the different chemical environments of the carbon atoms within the BOPHY core, i.e. C-C/C-H at 284.5 eV, C-I at 284.9, C-N at 285.1 eV and C=N at 285.8 eV. These results bring up two important conclusions: i) the I-BOPHY-I molecules arrive intact to the Au(111) surface with only a small fraction (16%) displaying a partial dehalogenation, probably due to molecular dehalogenation at more reactive surface sites (step edges and/or reconstruction elbows); ii) the amount of dehalogenated molecules inferred from the XPS analysis fits well with the proportion of metal-coordinated (I-BOPHY-Au-BOPHY-I) vs self-assembled nanostructures observed by STM, thus corroborating our models.

To fully activate the precursors, the I-BOPHY-I/Au(111) system was annealed at 370 K. Figure 2a and Figure S4 show STM images of the surface after the thermal treatment, where two phases coexist: i) linear molecular nanostructures self-assembled into islands, and ii) a surrounding nanoporous network. Figure 2b shows one of the islands, where elongated features are detected (green circle) together with rounded features of two different sizes (blue and red circles). From the image, it is possible to discern a periodicity along the elongated chain slabs of approximately 1.27 nm, in good agreement with half of the I-BOPHY-Au-BOPHY-I distance in the dimers detected at RT. Since each molecular row within the self-assembled island starts and ends with a rounded feature and taking into consideration the observed periodicity and the fact that it is not expected that the BOPHY molecule decomposes at 370 K, we propose the molecular model superimposed to the STM image in Figure 2c, corresponding to a (Au-BOPHY)$_n$ chain. This model, based on hybrid metal-organic chains on the Au(111) surface, assigns the center of the elongated feature to a gold surface adatom and fits perfectly with the characteristics observed when a defect is detected (see the molecular vacancy in the middle of the second upper molecular row). In that case, a rounded/elongated/rounded group is observed on both sides of the defect, which corresponds to a fully dehalogenated metal-organic dimer. This result indicates that the formation of BOPHY-based metal-organic oligomers originates by the thermal dehalogenation of the pristine molecules. Although one might expect the Ullmann reaction to occur by thermal activation, with the corresponding formation of a C-C covalent coupling between BOPHY molecules, that process does not take place, as inferred from the distance between chain slabs. The reason resides on the presence of the four voluminous terminal methyl groups, which prevent the formation of the C-C

bond due to steric effects. On the other hand, the small rounded features of the lower part of Figure 2b (red circles) are characteristic of atomic iodine, also present in the porous network surrounding the self-assembled islands, which is hardly distinguished in Figure 2a and better discerned in Figure S4b. These atoms, that after dehalogenation no longer bind to BOPHY molecules, remain on the surface forming a pseudo-hexagonal network on Au (111), as previously reported in the literature [30].

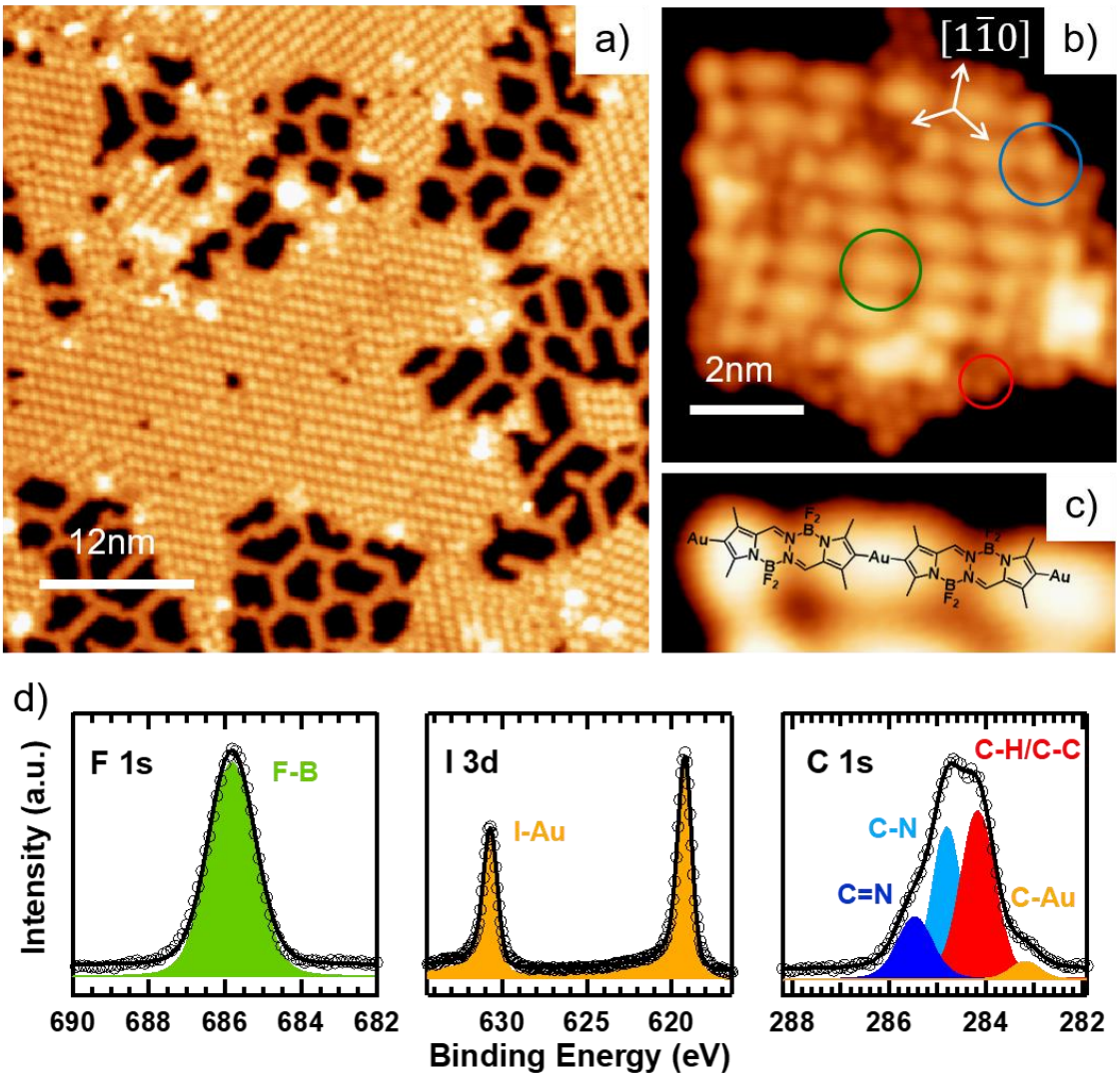

Figure 2. a) STM image after annealing the I-BOPHY-I/Au(111) sample at 370 K showing the molecular self-assembly and the porous regions. b) STM image of one self-assembled molecular island. The set of three white arrows show the main crystallographic directions of the Au(111) substrate. c) Representation of the proposed molecular model of BOPHY molecules coordinated with surface adatoms. d) XPS spectra corresponding to F 1s, I 3d and C 1s regions. STM parameters: a) I_t=0.05 nA, V_b=1 V; b) I_t=0.05 nA, V_b=0.5 V.

Figure 2d represents the corresponding F 1s, I 3d and C 1s XPS spectra. The F 1s signal does not change with respect to that of the RT phase, indicating that the fluorine atoms remain intact on the molecular backbone. This is not surprising, as it has been reported that F atoms remain attached to carbon-based molecular backbones at this temperature on Au(111) [31], and the C_6H_5-F bond is weaker than the BF-F bond present in BOPHYs (485 kJ/mol vs 523 kJ/mol) [32]. However, in the I 3d emission, the peak at 620.6 eV, associated to C-I, disappears, while only the peak at 619.3 eV, characteristic of chemisorbed I on the surface, remains, indicating the complete molecular dehalogenation. On the other hand, the C 1s XPS spectrum shows the vanishing of the C-I emission at 284.9 eV together with the development of a new component at 283.2 eV, typically assigned to C-metal bonds [33]. These XPS results confirm our previous hypothesis based on the STM images and evidence that, in the case of Au(111), the thermal treatment at 370 K leads to the complete dehalogenation of the I-BOPHY-I molecules and the formation of hybrid metal-organic chains.

To determine the influence of the molecular chirality in the growth of the oligomers, we have performed a statistical correlation analysis based on more than 900 molecules. This analysis evaluates whether there is any relationship between two variables, that is the two possible chiralities of the molecules along the oligomers. The value resulting from the analysis will range between 1 (total correlation, homochiral oligomers) and -1 (total correlation, heterochiral oligomers alternating both chiralities), with 0 indicating a complete uncorrelation (stochastic oligomers). The obtained value for our oligomers is -0.023, thus indicating the stochastic growth of the oligomers and pointing out the negligible role played by the chirality. This behavior is further corroborated by DFT

calculations, which indicate a similar total energy for homochiral and heterochiral polymers (ΔE = 0.13 eV).

Summarizing the results for the I-BOPHY-I molecules deposited on Au(111), two phases coexist at RT, the most extended one assigned to self-assembled I-BOPHY-I molecules and a minority phase of metal-organic dimers, I-BOPHY-Au-BOPHY-I, formed upon initial molecular dehalogenation. When the system is annealed at 370 K, the I-BOPHY-I molecules dehalogenate, inducing the formation of 1D metal-organic oligomers, (Au-BOPHY)$_n$ mediated by the native adatoms of the surface. Interestingly, the growth process is completely stochastic, with the molecular chirality playing no role in it.

<u>On Surface I-BOPHY-I chemistry at the Ag(111) metal interface</u>

As it can be observed in Figure 3a, the evaporation of I-BOPHY-I molecules on Ag(111) at RT already leads to the formation of linear chains, similar to those discerned on the Au(111) surface at 370 K. The STM image shows large and brighter islands of molecules forming a linear arrangement and, in the region between these islands, some small and darker aggregates. Within the molecular islands, it is possible to discern linear chains aligned along three different orientations, rotated by 120° among them, and oriented along the substrate [2-1-1] symmetry direction. To better identify the features constituting the linear chains, HR-STM images were recorded (see Figure 3b). The periodicity along chains is again around 1.3 nm, which suggests the presence of metal-organic I-BOPHY-Ag-BOPHY-I oligomers, already at RT, as a consequence of the complete dehalogenation of the molecules. Such results are not surprising, as a lower dehalogenation temperature on Ag(111) than on Au(111) has been previously reported [30]. The iodine atoms that are released from the BOPHY molecules upon the

dehalogenation process at RT form the small aggregates outside the striped molecular areas (see Figure 3a and Figure S5).

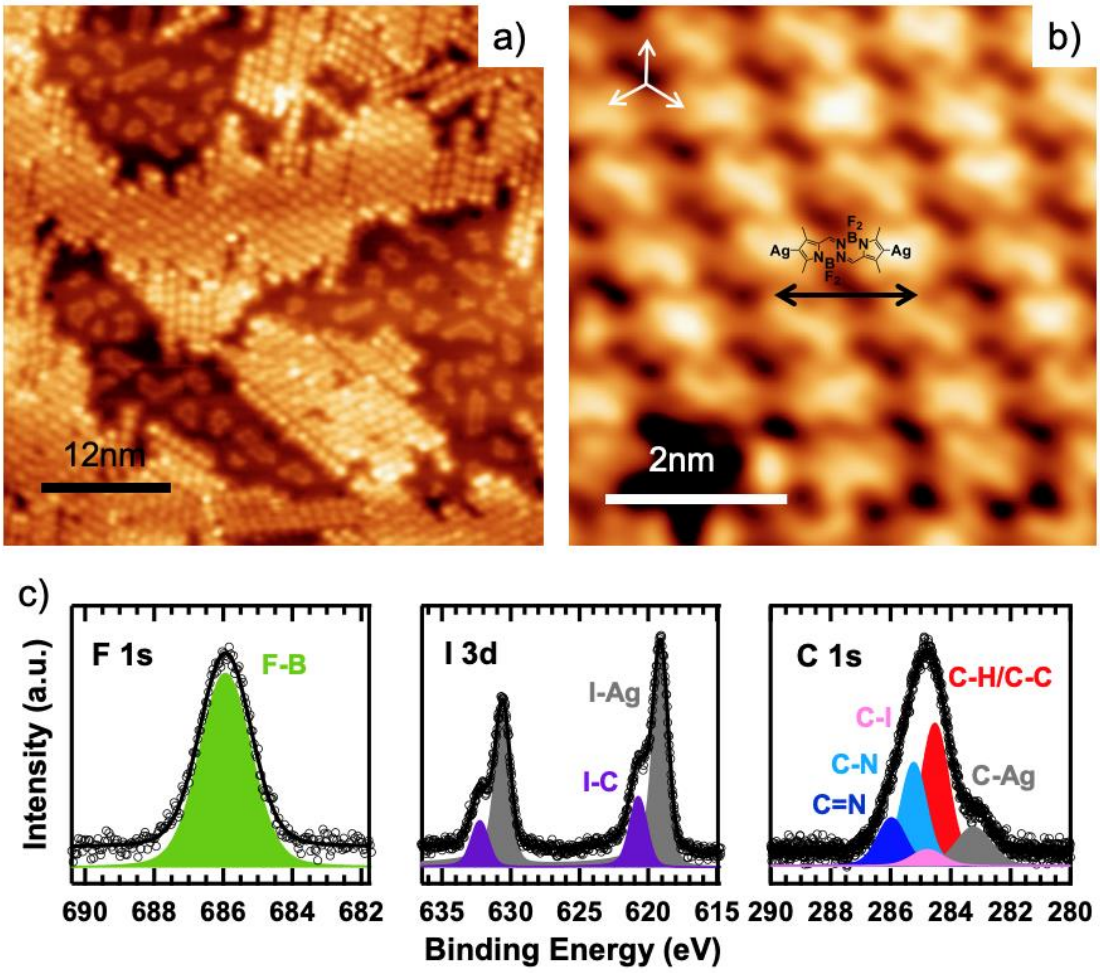

Figure 3. a) STM images after evaporation of I-BOPHY-I on Ag (111) at RT showing the molecular self-assembly surrounded by areas with iodine atoms. b) STM image of the self-assembly region. The set of three white arrows shows the [1-10] directions of the Ag(111) substrate. c) XPS spectra corresponding to F 1s, I 3d and C 1s regions. STM parameters: a) I_t=0.05 nA, V_b=1 V; b) I_t=0.05 nA, V_b=0.8 V.

Similarly, to the Au(111) case, the XPS characterization was used to reveal the chemical configuration of the molecular layer. Figure 3c shows the F 1s spectrum with the characteristic single component at 685.9 eV related to the B-F bond within the BOPHY core, together with the I 3d spectrum that presents a main peak at 619.0 eV (I-Ag) and a smaller one at 620.7 eV (I-C). It should be noted that it is well-known that iodinated molecules tend to undergo a complete dehalogenation already at RT on Ag(111) given

the more labile nature of the C-I bond with respect to the C-Br bond [34,35]. The incomplete dehalogenation observed here may be mostly ascribed to steric effects, where the present coverage, larger than that of STM images, inhibits further dehalogenation when molecules are trapped at surface regions already saturated by iodine atoms. Contribution to the I-C signal from second layer molecules is unlikely because this should give rise to a core level shift to higher binding energy of the corresponding F, N and C 1s peaks, which is not observed. The C 1s XPS spectrum confirms the formation of a C-Ag metal-organic bond at RT as inferred from the development of a component at 283.2 eV, as well as the dehalogenation of the majority of the molecules, with a residual minority C-I component at 284.8 eV. Thus, while on Au(111) the complete dehalogenation was taking place at 370 K, on Ag(111) this reaction is already achieved at RT. Similar results of molecular dehalogenation and formation of metal-organic nanostructures at RT have been reported in literature [35,36]. It should be noted that most of the halogenated molecules (> 60%) will contribute to the growth of the nanostructures upon annealing to 370 K, with only a small fraction desorbing from the surface (the total intensity of the I 3d spectrum after annealing is found to be 90% of that deposited at RT), see quantitative XPS analysis in Table S1 of ESI file.

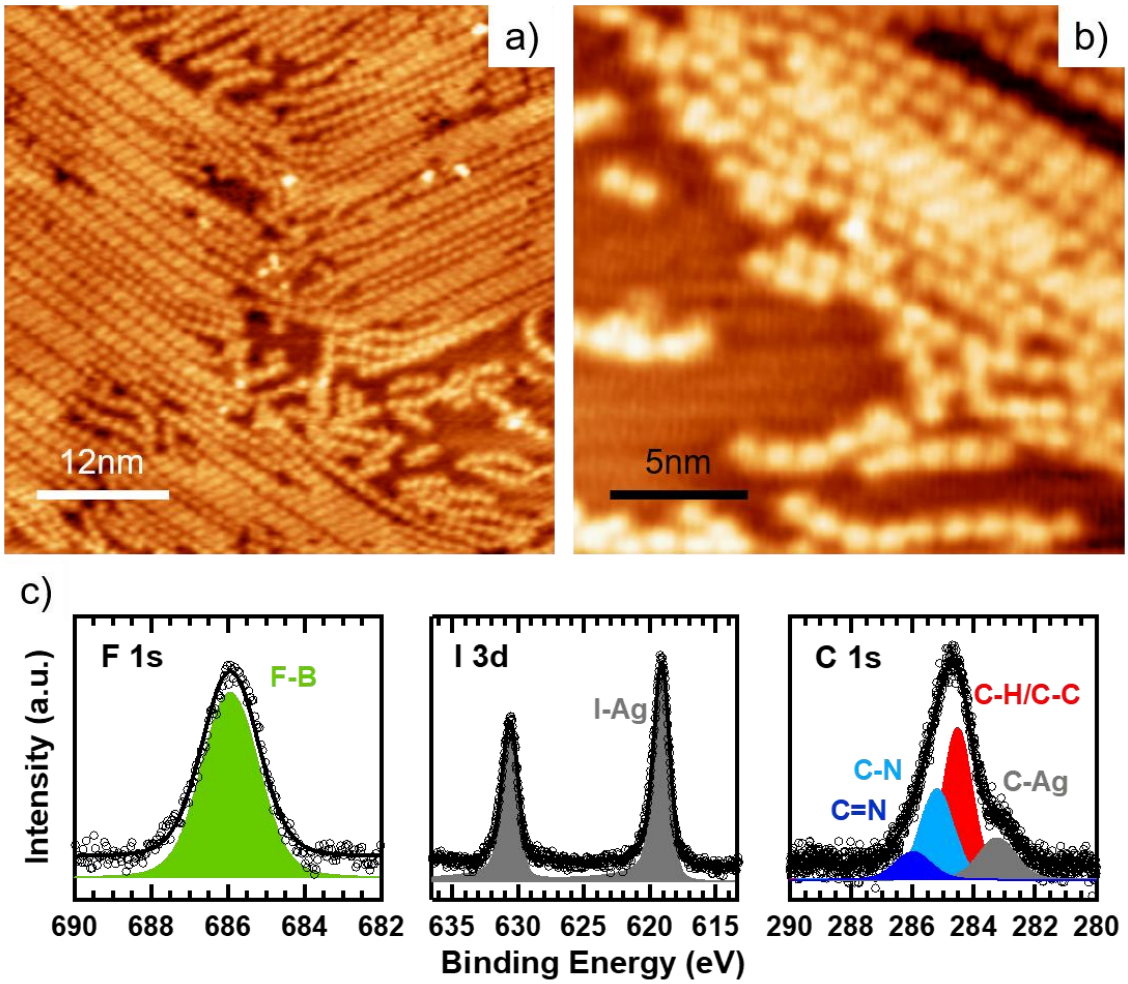

Figure 4. a) STM image after annealing the I-BOPHY-I/Ag (111) sample at 370 K, showing the linear molecular chains. b) STM image where the elongated slabs within the molecular chains are distinguished. c) XPS spectra corresponding to F 1s, I 3d and C 1s regions. STM parameters: a) I_t=0.05 nA, V_b=1 V; b) I_t=0.05 nA, V_b=1 V.

After post-annealing the BOPHY/Ag(111) sample at 370 K, longer molecular chains, $(BOPHY\text{-}Ag)_n$, are formed (see Figure 4a), whose elongated slabs can be better appreciated in the STM image of Figure 4b. The periodicity between monomers does not change with respect to the RT phase, indicating that only the length of the BOPHY-based metal-organic oligomers has changed. As it is shown in the XPS spectra of Figure 4c, upon annealing the system at 370 K, the I-C signal in both C 1s and I 3d emissions disappears, while the C-Ag component increases its intensity from 12% (at RT) to 16% (at 370 K), in excellent agreement with the total activation of the I-BOPHY-I molecules.

This result indicates a total dehalogenation of the I-BOPHY-I molecules on the surface. Additionally, the shape of F 1s XPS peak does not change after post-annealing, confirming the stability of the molecule on the surface.

To analyze the influence of the substrate, Au(111) or Ag(111), on the length of the oligomers after annealing at 370 K, we have performed a statistical analysis over more than 370 oligomers (Figure 5). From the histograms, it can be appreciated that the oligomers on Ag(111) are, on average, two times longer than on Au(111) for a similar coverage. This result can be attributed to several factors, such as the higher availability of surface adatoms on Ag(111) [37,38], which may promote the generation of longer chains; the presence of the herringbone reconstruction on the Au(111) surface, which could limit the oligomer length; and the surrounding iodine network around the oligomer islands on Au(111), which could hinder the molecular diffusion and the formation of longer oligomers.

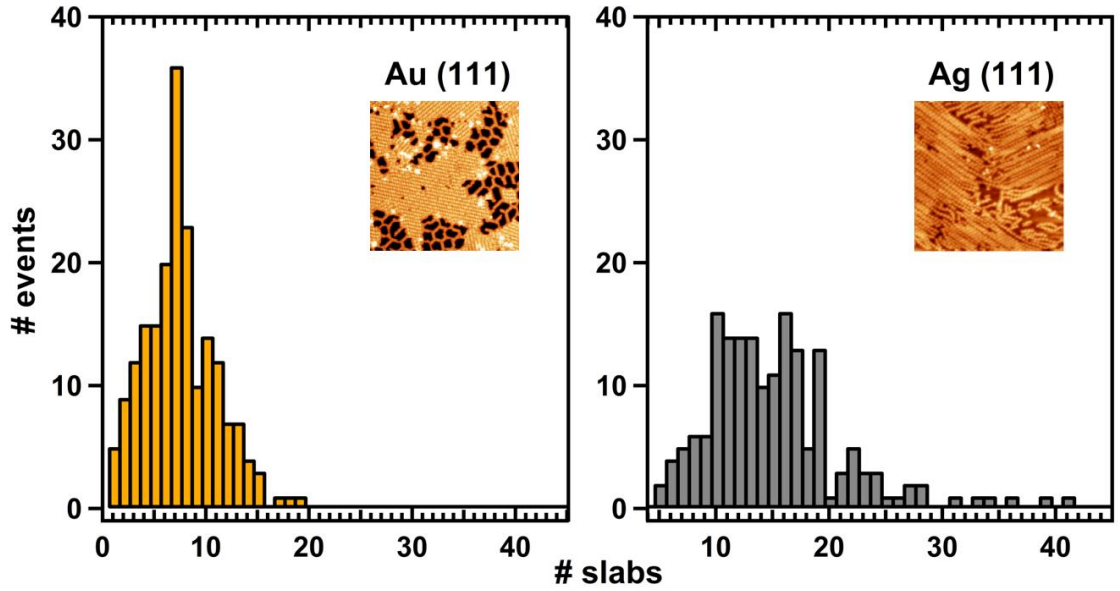

Figure 5. Histograms representing the number of events as a function of the number of slabs per chain on the metal surface after annealing at 370 K: a) for Au(111) and b) for Ag(111) substrates.

Air stability

As it has been already introduced, BOPHY molecules are excellent photoactive molecules for the development of improved photoelectrodes. Thus, the so-formed high quality BOPHY-based metal-organic oligomers could be of great interest in photo(electro)catalytic applications. However, these are prepared under ideal UHV conditions, far from real applications. If these nanostructures are to be applied, it becomes crucial to investigate, first of all, their air-stability (usually known as *bridging the pressure gap*). For this purpose, we have followed the air stability of these oligomers on both substrates, Au(111) and Ag(111), by XPS, acquiring spectra before and after a 10 min exposure to air and a subsequent post-annealing at 370 K to desorb possible physisorbed contaminants and check the stability of the products.

Figure 6a shows the O 1s and C 1s XPS spectra for both samples after a 10 minutes air exposure and with subsequent annealing at 370 K for 15 min. In the case of the oligomers synthesized in vacuum at 370 K on Au(111), the C 1s spectrum after air exposure (middle spectra in graph) is very similar to the one obtained before the exposure (bottom spectra), indicating that the oligomers preserve their integrity. Interestingly, it is still possible to discern the C-Au peak (yellow curve) associated to the metal-organic oligomers. Their integrity is further supported by the absence of an O peak (left side, orange curves), which it is well-known to be the most reactive species when organic structures are exposed to air [7]. To confirm the integrity of the oligomers and their stability, the exposed sample was further annealed at 370 K (top spectra), resulting in a C 1s spectrum almost identical to that obtained before the annealing.

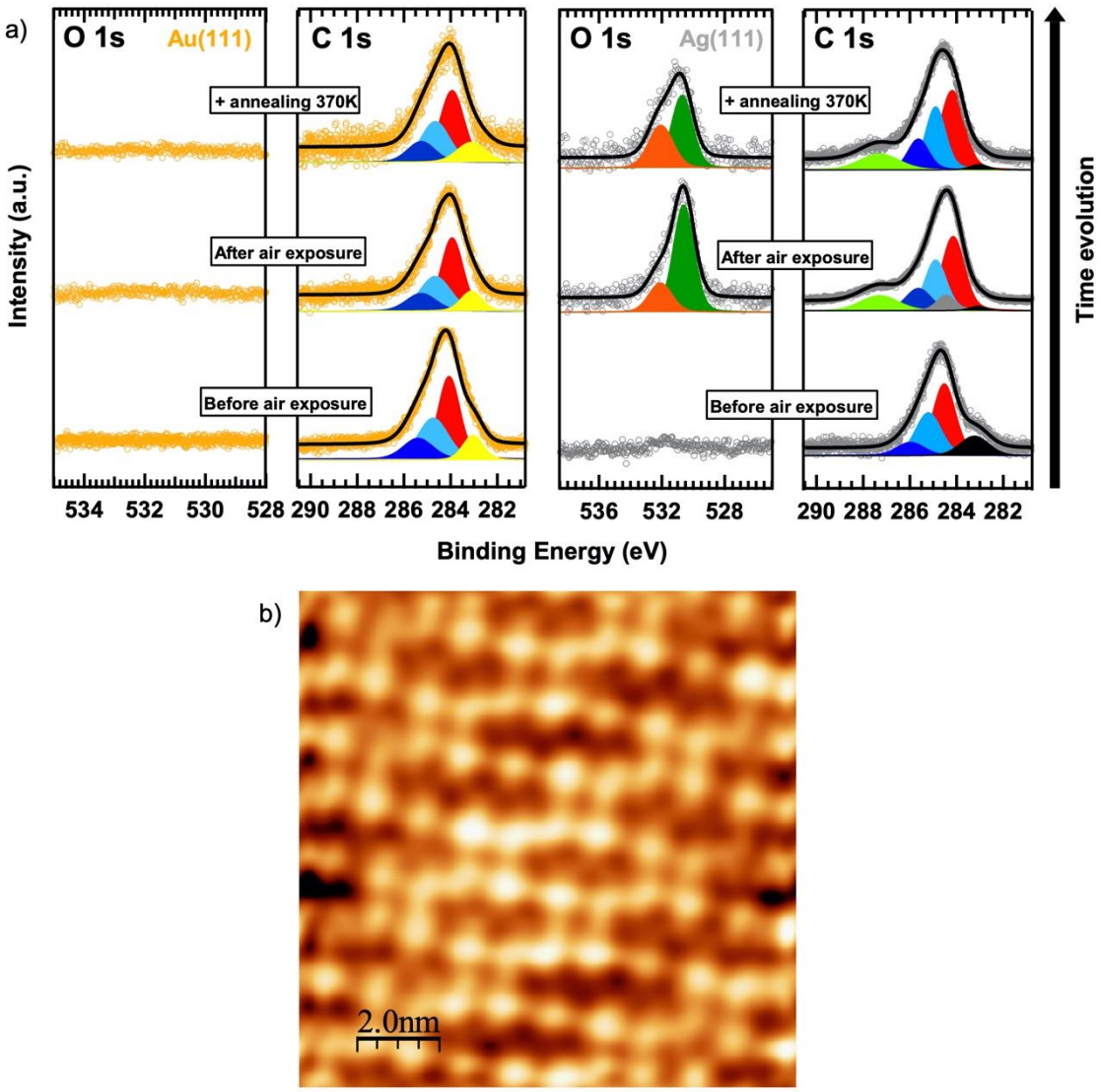

Figure 6. a) XPS O 1s (left) and C 1s (right) spectra of BOPHY-based oligomers on Au(111) (top orange curves) and Ag(111) (bottom grey curves) for the different steps of the air exposure. b) STM image of the air-exposed BOPHY/Ag(111) sample. STM parameters: I_t=0.1 nA, V_b=1 V.

The Ag(111) case is interestingly different: upon air exposure, both the O 1s and C 1s peaks change. In the former case, we see the appearance of an O 1s emission composed of two contributions located at 530.5 eV and 532.0 eV. The one at lower BE is assigned to AgO and physisorbed O_2, in good agreement with literature [39,40], while the one at higher BE is compatible with oxygen species bonded to organic C [41]. Furthermore, two important changes occur in the C 1s spectrum. The first one is the almost complete disappearance of the C-Ag component (black curve at 283.1 eV). The second one is the

appearance of a new component at 287.3 eV (light green curve), which is consistent with the formation of carbon-oxygen bonds, in accordance with the result obtained for the O 1s peak. Thus, both results indicate the rupture of the metal-organic oligomers and the possible stabilization of the system with the incorporation of oxygen-containing species. The STM results of the air-exposed BOPHY/Ag(111) sample show a transformation in the oligomers from linear structures into kinked ones, with a periodicity of around 1.1 nm (Figure 6b), which again could indicate the formation of covalent BOPHY-based oligomers. To better understand this process, we have performed DFT-based calculations on different possible scenarios considering the XPS results and some of the most abundant oxygen-containing species present in air (Figure S8). The initial case where the BOPHY molecules are coordinated to Ag atoms presents an energy stored at the C-Ag bonds of -1.64 eV. If we consider the displacement of the Ag atom by a CO molecule, the resulting structure would present an energy gain of 0.84 eV (C-CO bond energy of -2.48 eV). On the other hand, if the Ag atom were replaced by an oxygen atom, the bond energy would increase to -3.20 eV, making it the most stable situation. Thus, our DFT results suggest the unexpected formation of ether-bridged covalent oligomers upon exposure to air. It must be noted that the incorporation of this extra atom in between BOPHY molecules separates the molecules enough so that they do not feel the steric repulsion between the methyl groups, allowing for the covalent bonding between them.

At this point, it is interesting to analyze the possible mechanism yielding the formation of such structures by the incorporation of atomic oxygen into the oligomers. The first step has to be the formation of atomic oxygen by the dissociation of molecular oxygen on the surface. It has been reported that O_2 adsorption on Au(111) presents a very low

yield [42], being necessary to add atomic O to improve such adsorption, while O_2 readily dissociates on a silver surface [43]. To confirm this point, we have carried out a theoretical estimation of the dissociation barriers for O_2 on both substrates, yielding values of 1.26 eV for Ag(111) and 1.90 eV and Au(111), in excellent agreement with previous theoretical findings [44,45]. Consequently, the dissociation of molecular O_2 on Au(111) is expected to be nearly negligible whereas it remains feasible on Ag(111). The second step would correspond to the replacement of the metallic center by the atomic oxygen. Our DFT results indicate that the stability of the Au metal-organic oligomers is higher than those stabilized by Ag atoms (-2.19 eV vs -1.64 eV, respectively), making more difficult for the oxygen atom to displace the metallic center. Thus, the following scenario can be envisioned: when molecular oxygen reaches the Ag(111) surface at RT, it dissociates into atomic oxygen that it is available to displace the metal adatom in the oligomers, while this process is quenched on Au(111). To analyze the stability of such phase and to confirm our hypothesis, we have post-annealed the exposed surface to 370 K. The C 1s spectrum is preserved, with the only difference of the disappearance of the grey component at 284.5 eV that is assigned to carbon contaminants physisorbed on the surface. The O 1s peak also keeps its two components although the one at 530.5 eV is significantly reduced. This can be easily understood if we notice that this component has a double contribution, AgO and physisorbed O_2, and that the second one can desorb upon annealing, thus remaining the one associated to AgO, which is known to desorb at temperatures above 500 K [46].

The XPS peaks corresponding to the other elements exhibit the same number of components with a relatively similar shape before and after exposure to air (see Figures S6 and S7). Consequently, these results confirm the low stability of the oligomers

synthesized on Ag(111) and the preservation of those formed on Au(111), whose chemical stability in air paves the way for the development of photoactive materials with low dimensionality through on-surface synthesis.

Conclusions

In this work, the influence of the substrate on the formation and air stability of metal-organic oligomers on Au(111) and Ag(111) from photoactive I-BOPHY-I molecules has been investigated. A multi-technique analysis combining STM and XPS, and supported by DFT theoretical calculations, allows for a comprehensive characterization from the structural and chemical points of view. On Au(111), typically being the most inert surface, the intact I-BOPHY-I molecules are mostly arranged into a linear self-assembly although a minority phase formed by BOPHY-based dimers is also observed at RT. At 370 K, the molecules are completely dehalogenated and form extended compact islands of chains through surface adatoms. On Ag(111), most molecules undergo a complete dehalogenation at the surface already at RT, resulting in the formation of BOPHY-based oligomers at this temperature. When the temperature is increased to 370 K, longer chains are obtained on this surface as compared to the Au(111) one. Additionally, the air stability of the oligomers has been tested, as a first step toward applications, being more stable on Au(111) than on Ag(111), where a transformation of metal-organic into ether-bridged BOPHY-based oligomers occurs. This research highlights the opportunity to develop low-dimensional photoactive materials that are promising for practical applications and the crucial role that the supporting substrates can play not only in the formation of the nanostructures but also in their air stability and integrity.

Acknowledgements

This work was supported by the S2018/NMT-4367, Y2020/NMT-6469, TEC-2024/TEC-308 and TEC-2024/TEC-459 projects funded by the “Comunidad de Madrid” and co-financed by European Structural Funds, and by grants PID2020-113142RB-C21, PID2023-146801NB-C33, PID2023-149077OB-C31, PID2021-12509OA-I00, TED2021-129999B-C31, TED2021-129416A-I00, PLEC2021-007906 and RED2022-134503-T funded by MCIN/AEI/10.13039/501100011033 and by “ERDF A way of making Europe”, by “ERDF/EU” and the “European Union NextGenerationEU/ PRTR”.

References:

[1] S. Clair, D.G. de Oteyza, Controlling a Chemical Coupling Reaction on a Surface: Tools and Strategies for On-Surface Synthesis, Chem. Rev. 119 (2019) 4717–4776. https://doi.org/10.1021/acs.chemrev.8b00601.

[2] J. Méndez, M. Francisca López, J. A. Martín-Gago, On-surface synthesis of cyclic organic molecules, Chemical Society Reviews 40 (2011) 4578–4590. https://doi.org/10.1039/C0CS00161A.

[3] T. Wang, J. Zhu, Confined on-surface organic synthesis: Strategies and mechanisms, Surface Science Reports 74 (2019) 97–140. https://doi.org/10.1016/j.surfrep.2019.05.001.

[4] G. Borin Barin, Q. Sun, M. Di Giovannantonio, C.-Z. Du, X.-Y. Wang, J.P. Llinas, Z. Mutlu, Y. Lin, J. Wilhelm, J. Overbeck, C. Daniels, M. Lamparski, H. Sahabudeen, M.L. Perrin, J.I. Urgel, S. Mishra, A. Kinikar, R. Widmer, S. Stolz, M. Bommert, C. Pignedoli, X. Feng, M. Calame, K. Müllen, A. Narita, V. Meunier, J. Bokor, R. Fasel, P. Ruffieux, Growth Optimization and Device Integration of Narrow-Bandgap Graphene Nanoribbons, Small 18 (2022) 2202301. https://doi.org/10.1002/smll.202202301.

[5] M. Tenorio, C. Moreno, P. Febrer, J. Castro-Esteban, P. Ordejón, D. Peña, M. Pruneda, A. Mugarza, Atomically Sharp Lateral Superlattice Heterojunctions Built-In Nitrogen-Doped Nanoporous Graphene, Advanced Materials 34 (2022) 2110099. https://doi.org/10.1002/adma.202110099.

[6] B. Wurster, D. Grumelli, D. Hötger, R. Gutzler, K. Kern, Driving the Oxygen Evolution Reaction by Nonlinear Cooperativity in Bimetallic Coordination Catalysts, J. Am. Chem. Soc. 138 (2016) 3623–3626. https://doi.org/10.1021/jacs.5b10484.

[7] J. Lawrence, A. Berdonces-Layunta, S. Edalatmanesh, J. Castro-Esteban, T. Wang, A. Jimenez-Martin, B. de la Torre, R. Castrillo-Bodero, P. Angulo-Portugal, M.S.G. Mohammed, A. Matěj, M. Vilas-Varela, F. Schiller, M. Corso, P. Jelinek, D. Peña, D.G. de Oteyza, Circumventing the stability problems of graphene nanoribbon zigzag edges, Nat. Chem. 14 (2022) 1451–1458. https://doi.org/10.1038/s41557-022-01042-8.

[8] I.-S. Tamgho, A. Hasheminasab, J.T. Engle, V.N. Nemykin, C.J. Ziegler, A New Highly Fluorescent and Symmetric Pyrrole–BF2 Chromophore: BOPHY, J. Am. Chem. Soc. 136 (2014) 5623–5626. https://doi.org/10.1021/ja502477a.

[9] C. Yu, L. Jiao, P. Zhang, Z. Feng, C. Cheng, Y. Wei, X. Mu, E. Hao, Highly Fluorescent BF2 Complexes of Hydrazine–Schiff Base Linked Bispyrrole, Org. Lett. 16 (2014) 3048–3051. https://doi.org/10.1021/ol501162f.

[10] E. Tunca, E. Teknikel, C. Unaleroglu, An Unprecedented Reaction of BOPHY: Fluorimetric Chemosensing of Amines by Tetrabrominated BOPHY, ChemistrySelect 9 (2024) e202304490. https://doi.org/10.1002/slct.202304490.

[11] X.-D. Jiang, Y. Su, S. Yue, C. Li, H. Yu, H. Zhang, C.-L. Sun, L.-J. Xiao, Synthesis of mono-(p-dimethylamino)styryl-containing BOPHY dye for a turn-on pH sensor, RSC Adv. 5 (2015) 16735–16739. https://doi.org/10.1039/C4RA15914D.

[12] C. He, H. Zhou, N. Yang, N. Niu, E. Hussain, Y. Li, C. Yu, A turn-on fluorescent BOPHY probe for Cu2+ ion detection, New J. Chem. 42 (2018) 2520–2525. https://doi.org/10.1039/C7NJ03911E.

[13] E.J. Gonzalez Lopez, A.M. Sarotti, S.R. Martínez, L.P. Macor, J.E. Durantini, M. Renfige, M.A. Gervaldo, L.A. Otero, A.M. Durantini, E.N. Durantini, D.A. Heredia, BOPHY-Fullerene C60 Dyad as a Photosensitizer for Antimicrobial Photodynamic Therapy, Chemistry – A European Journal 28 (2022) e202103884. https://doi.org/10.1002/chem.202103884.
[14] F. Lv, D. Liu, W. Zheng, Y. Zhao, F. Song, BOPHY-Based Aggregation-Induced-Emission Nanoparticle Photosensitizers for Photodynamic Therapy, ACS Appl. Nano Mater. 4 (2021) 6012–6019. https://doi.org/10.1021/acsanm.1c00862.
[15] O.J. Woodford, R. Ziessel, A. Harriman, Photofading of an Extended BOPHY Chromophore Dispersed in Poly(methyl methacrylate) as a Chemical Actinometer, ChemPhotoChem 2 (2018) 1046–1054. https://doi.org/10.1002/cptc.201800130.
[16] C.G. López-Calixto, M. Liras, V.A. de la Peña O'Shea, R. Pérez-Ruiz, Synchronized biphotonic process triggering CC coupling catalytic reactions, Applied Catalysis B: Environmental 237 (2018) 18–23. https://doi.org/10.1016/j.apcatb.2018.05.062.
[17] C.G. López-Calixto, S. Cabrera, R. Pérez-Ruiz, M. Barawi, J. Alemán, V.A. de la Peña O'Shea, M. Liras, Conjugated porous polymer based on BOPHY dyes as photocatalyst under visible light, Applied Catalysis B: Environmental 258 (2019) 117933. https://doi.org/10.1016/j.apcatb.2019.117933.
[18] C.G. López-Calixto, M. Barawi, M. Gomez-Mendoza, F.E. Oropeza, F. Fresno, M. Liras, V.A. de la Peña O'Shea, Hybrids Based on BOPHY-Conjugated Porous Polymers as Photocatalysts for Hydrogen Production: Insight into the Charge Transfer Pathway, ACS Catal. 10 (2020) 9804–9812. https://doi.org/10.1021/acscatal.0c01346.
[19] L. Collado, T. Naranjo, M. Gomez-Mendoza, C.G. López-Calixto, F.E. Oropeza, M. Liras, J. Marugán, V.A. de la Peña O'Shea, Conjugated Porous Polymers Based on BODIPY and BOPHY Dyes in Hybrid Heterojunctions for Artificial Photosynthesis, Advanced Functional Materials 31 (2021) 2105384. https://doi.org/10.1002/adfm.202105384.
[20] T. Mazuelo, T. Naranjo, M. Gomez-Mendoza, A.H. Pizarro, L. Collado, M. Barawi, F. Gándara, M. Liras, V.A. de la P. O'Shea, A covalent organic framework based on BOPHY/TiO2 hybrid photocatalysts for solar driven hydrogen production, J. Mater. Chem. A 12 (2024) 1476–1487. https://doi.org/10.1039/D3TA06314C.
[21] F. Suárez-Blas, M. Martínez-Fernández, A. Prieto-Castañeda, A. García-Fernández, J.I. Martínez, M.M. Ramos, M.J. Ortiz, R. Martínez-Máñez, J.L. Segura, BODIPY doping of covalent organic frameworks-based nanomaterials: A novel strategy towards biomedical applications, Dyes and Pigments 219 (2023) 111561. https://doi.org/10.1016/j.dyepig.2023.111561.
[22] M. Buyuktemiz, M. Kılıç, Y. Che, J. Zhao, Y. Dede, When Does Fusing Two Rings Not Yield a Larger Ring? The Curious Case of BOPHY, J. Org. Chem. 86 (2021) 4547–4556. https://doi.org/10.1021/acs.joc.0c02976.
[23] O. Stetsovych, M. Švec, J. Vacek, J.V. Chocholoušová, A. Jančařík, J. Rybáček, K. Kosmider, I.G. Stará, P. Jelínek, I. Starý, From helical to planar chirality by on-surface chemistry, Nature Chem 9 (2017) 213–218. https://doi.org/10.1038/nchem.2662.
[24] I. Horcas, R. Fernández, J.M. Gómez-Rodríguez, J. Colchero, J. Gómez-Herrero, A.M. Baro, WSXM: A software for scanning probe microscopy and a tool for

nanotechnology, Review of Scientific Instruments 78 (2007) 013705. https://doi.org/10.1063/1.2432410.
[25] L. Floreano, A. Cossaro, R. Gotter, A. Verdini, G. Bavdek, F. Evangelista, A. Ruocco, A. Morgante, D. Cvetko, Periodic Arrays of Cu-Phthalocyanine Chains on Au(110), J. Phys. Chem. C 112 (2008) 10794–10802. https://doi.org/10.1021/jp711140e.
[26] M.J. Frisch, G.W. Trucks, H.B. Schlegel, G.E. Scuseria, M.A. Robb, J.R. Cheeseman, G. Scalmani, V. Barone, G.A. Petersson, H. Nakatsuji, X. Li, M. Caricato, A.V. Marenich, J. Bloino, B.G. Janesko, R. Gomperts, B. Menucci, H.P. Hratchian, J.V. Ortiz, A.F. Izmaylov, J.L. Sonnenberg, D. Williams-Young, F. Ding, F. Lipparini, F. Egidi, J. Goings, B. Peng, A. Petrone, T. Henderson, D. Ranasinghe, V.G. Zakrzewski, J. Gao, N. Rega, G. Zheng, W. Liang, M. Hada, M. Ehara, K. Toyota, R. Fukuda, J. Hasegawa, M. Ishida, T. Nakajima, Y. Honda, O. Kitao, H. Nakai, T. Vreven, K. Throssell, J.A. Montgomery, J.E. Peralta, F. Ogliaro, M.J. Bearpark, J.J. Heyd, E.N. Brothers, K.N. Kudin, V.N. Staroverov, T.A. Keith, R. Kobayashi, J. Normand, K. Raghavachari, A.P. Rendell, J.C. Burant, S.S. Iyengar, J. Tomasi, M. Cossi, J.M. Millam, M. Klene, C. Adamo, R. Cammi, J.W. Ochterski, R.L. Martin, K. Morokuma, O. Farkas, J.B. Foresman, D.J. Fox, Gaussian16 R.C01, (2016).
[27] P. Giannozzi, S. Baroni, N. Bonini, M. Calandra, R. Car, C. Cavazzoni, D. Ceresoli, G.L. Chiarotti, M. Cococcioni, I. Dabo, A.D. Corso, S. de Gironcoli, S. Fabris, G. Fratesi, R. Gebauer, U. Gerstmann, C. Gougoussis, A. Kokalj, M. Lazzeri, L. Martin-Samos, N. Marzari, F. Mauri, R. Mazzarello, S. Paolini, A. Pasquarello, L. Paulatto, C. Sbraccia, S. Scandolo, G. Sclauzero, A.P. Seitsonen, A. Smogunov, P. Umari, R.M. Wentzcovitch, QUANTUM ESPRESSO: a modular and open-source software project for quantum simulations of materials, J. Phys.: Condens. Matter 21 (2009) 395502. https://doi.org/10.1088/0953-8984/21/39/395502.
[28] J.P. Lewis, P. Jelínek, J. Ortega, A.A. Demkov, D.G. Trabada, B. Haycock, H. Wang, G. Adams, J.K. Tomfohr, E. Abad, H. Wang, D.A. Drabold, Advances and applications in the FIREBALL ab initio tight-binding molecular-dynamics formalism, Physica Status Solidi (b) 248 (2011) 1989–2007. https://doi.org/10.1002/pssb.201147259.
[29] C. Li, C. Yin, X. Mu, J. Maier, Top-Down Synthesis of Open Framework Fluoride for Lithium and Sodium Batteries, Chem. Mater. 25 (2013) 962–969. https://doi.org/10.1021/cm304127c.
[30] M. Di Giovannantonio, O. Deniz, J.I. Urgel, R. Widmer, T. Dienel, S. Stolz, C. Sánchez-Sánchez, M. Muntwiler, T. Dumslaff, R. Berger, A. Narita, X. Feng, K. Müllen, P. Ruffieux, R. Fasel, On-Surface Growth Dynamics of Graphene Nanoribbons: The Role of Halogen Functionalization, ACS Nano 12 (2018) 74–81. https://doi.org/10.1021/acsnano.7b07077.
[31] H. Hayashi, J. Yamaguchi, H. Jippo, R. Hayashi, N. Aratani, M. Ohfuchi, S. Sato, H. Yamada, Experimental and Theoretical Investigations of Surface-Assisted Graphene Nanoribbon Synthesis Featuring Carbon–Fluorine Bond Cleavage, ACS Nano 11 (2017) 6204–6210. https://doi.org/10.1021/acsnano.7b02316.
[32] N.A. Lange, Lange's handbook of chemistry, 15. ed, McGraw-Hill, New York, NY, 1999.
[33] I.R. Márquez, N. Ruíz del Árbol, J.I. Urgel, F. Villalobos, R. Fasel, M.F. López, J.M. Cuerva, J.A. Martín-Gago, A.G. Campaña, C. Sánchez-Sánchez, On-Surface Thermal Stability of a Graphenic Structure Incorporating a Tropone Moiety, Nanomaterials 12 (2022) 488. https://doi.org/10.3390/nano12030488.

[34] M. Lischka, M. Fritton, J. Eichhorn, V.S. Vyas, T. Strunskus, B.V. Lotsch, J. Björk, W.M. Heckl, M. Lackinger, On-Surface Polymerization of 1,6-Dibromo-3,8-diiodpyrene—A Comparative Study on Au(111) Versus Ag(111) by STM, XPS, and NEXAFS, J. Phys. Chem. C 122 (2018) 5967–5977. https://doi.org/10.1021/acs.jpcc.7b10403.
[35] C.J. Judd, S.L. Haddow, N.R. Champness, A. Saywell, Ullmann Coupling Reactions on Ag(111) and Ag(110); Substrate Influence on the Formation of Covalently Coupled Products and Intermediate Metal-Organic Structures, Sci Rep 7 (2017) 14541. https://doi.org/10.1038/s41598-017-13315-1.
[36] H. Lu, E. Wenlong, Z. Ma, X. Yang, Organometallic polymers synthesized from prochiral molecules by a surface-assisted synthesis on Ag(111), Phys. Chem. Chem. Phys. 22 (2020) 8141–8145. https://doi.org/10.1039/C9CP06893G.
[37] G. Boisvert, Energetics of diffusion on the (100) and (111) surfaces of Ag, Au, and Ir from first principles, Phys. Rev. B 52 (1995) 9078–9085. https://doi.org/10.1103/PhysRevB.52.9078.
[38] G. Boisvert, L.J. Lewis, Self-diffusion on low-index metallic surfaces: Ag and Au (100) and (111), Phys. Rev. B 54 (1996) 2880–2889. https://doi.org/10.1103/PhysRevB.54.2880.
[39] V.K. Kaushik, XPS core level spectra and Auger parameters for some silver compounds, Journal of Electron Spectroscopy and Related Phenomena 56 (1991) 273–277. https://doi.org/10.1016/0368-2048(91)85008-H.
[40] V.I. Bukhtiyarov, V.V. Kaichev, I.P. Prosvirin, Oxygen adsorption on Ag(111): X-ray photoelectron spectroscopy (XPS), angular dependent x-ray photoelectron spectroscopy (ADXPS) and temperature-programmed desorption (TPD) studies, The Journal of Chemical Physics 111 (1999) 2169–2175. https://doi.org/10.1063/1.479488.
[41] G.P. López, D.G. Castner, B.D. Ratner, XPS O 1s binding energies for polymers containing hydroxyl, ether, ketone and ester groups, Surface and Interface Analysis 17 (1991) 267–272. https://doi.org/10.1002/sia.740170508.
[42] X. Deng, B.K. Min, A. Guloy, C.M. Friend, Enhancement of O2 Dissociation on Au(111) by Adsorbed Oxygen: Implications for Oxidation Catalysis, J. Am. Chem. Soc. 127 (2005) 9267–9270. https://doi.org/10.1021/ja050144j.
[43] C.T. Campbell, Atomic and molecular oxygen adsorption on Ag(111), Surface Science 157 (1985) 43–60. https://doi.org/10.1016/0039-6028(85)90634-X.
[44] J.L.C. Fajín, M.N.D.S. Cordeiro, J.R.B. Gomes, DFT study on the reaction of O2 dissociation catalyzed by gold surfaces doped with transition metal atoms, Applied Catalysis A: General 458 (2013) 90–102. https://doi.org/10.1016/j.apcata.2013.03.023.
[45] H. Xin, S. Linic, Analyzing relationships between surface perturbations and local chemical reactivity of metal sites: Alkali promotion of O2 dissociation on Ag(111), The Journal of Chemical Physics 144 (2016) 234704. https://doi.org/10.1063/1.4953906.
[46] B.V. Andryushechkin, V.M. Shevlyuga, T.V. Pavlova, G.M. Zhidomirov, K.N. Eltsov, Adsorption of molecular oxygen on the Ag(111) surface: A combined temperature-programmed desorption and scanning tunneling microscopy study, The Journal of Chemical Physics 148 (2018) 244702. https://doi.org/10.1063/1.5037169.